Electron degradation and yields of initial products: V. Degradation spectra, the ionization yield, and the Fano factor for argon under electron irradiation

Ken-ichi Kowari, Mineo Kimura, and Mitio Inokuti
Argonne National Laboratory, Argonne, Illinois 60439
(Received 31 October 1988; revised manuscript received 27 December 1988)

The electron-degradation spectrum is fundamental for describing a variety of quantities bearing on electron slowing-down processes in matter. We calculate the electron-degradation spectrum in Ar gas by solving the Spencer-Fano equation, using a realistic set of cross sections. The influence of Auger electrons on the degradation spectrum is studied in detail. As an application, we study the statistical fluctuations in the ionization yield, which are expressed in terms of the Fano factor $F(T)$ for an electron incident at fixed energy T. The energy dependence of $F(T)$ is greatly influenced by L-shell ionization. The Fano factor approaches an asymptotic value of 0.16 at $T=2$ keV. Our results are consistent with experimental results.

INTRODUCTION

When an energetic electron enters matter, it interacts with atoms and molecules. As a result of a series of inelastic collisions of the primary and secondary electrons with constituent atoms and molecules in matter, excited states and ion pairs are produced. Evaluation of the yields of ions and of excited states is essential as a basis of dosimetry, radiation chemistry, and biology. There are two approaches to the calculation of the yields. One is the Monte Carlo method, which has been applied to the electron degradation in Ar by Unnikrishnan and Prasad,[1] by Parikh,[2] and by Grosswendt.[3] The other is the analytic transport theory that uses the Spencer-Fano equation,[4–7] which is the theme of the present work. Whereas the Monte Carlo method is straightforward to perform on a computer (and is also readily applicable to complicated problems such as those involving the spatial distribution of electron tracks), the analytic theory often provides a more transparent insight into the physics. Thus the two approaches are complementary rather than competitive.

In the analytic theory several avenues exist for the calculation of yields of initial products. (By the term "initial products" we mean here ions, excited states, dissociation fragments, and other molecular species that are formed *immediately following electron collisions and degradation.* This usage is different from that of radiation chemists, in which initial products mean the species that signals the initial condition for diffusion and chemical kinetics; the initial condition here refers to a much later time than electron degradation.) Direct calculation is possible by the solution of the Fowler equation, as was carried out for Ar by Eggarter,[8] who also determined a comprehensive set of realistic cross sections. Eggarter[9] later extended the calculation to the ionization yields in Ar-H_2 mixtures. Studies on the mixtures were further extended by Kimura and Inokuti,[10] who evaluated the yields of various excited states. Another avenue of study is seen in the work of Prasad and Unnikrishnan,[11] who solved for Ar the equation of Knipp *et al.*[12] for the probability of the production of a precise number of ions as a result of complete electron degradation. By far the most effective avenue is the solution of the Spencer-Fano equation for the electron degradation spectrum (or the track-length distribution), as is seen from the discussions in Refs. 5–7.

The purpose of the present article is to report the electron degradation spectra in Ar obtained by solving the Spencer-Fano equation[13] for a variety of situations. Applications include calculations of the ionization yield and of its statistical fluctuations as characterized by the Fano factor, defined as the ratio of the variance $D(T)$ to the mean number $N_i(T)$ of ions resulting from the complete degradation of an electron of initial kinetic energy T,

$$F(T)=D(T)/N_i(T) . \tag{1}$$

As input to the calculations we use the set of cross-section data determined by Eggarter[8] and fully documented by Eggarter and Inokuti.[14] The effects of both M-shell and L-shell ionizations are included in the calculations. Auger electrons following the L-shell ionization are specifically treated.

THEORY

For the simplest medium consisting of atoms or molecules with a single ionization threshold, the Spencer-Fano equation, the Fowler equation, and other related expressions have been described in detail in Refs. 5–7. We extend the treatment to the case of many ionization thresholds.

The Spencer-Fano equation

Let $y(T)dT$ represent the total path length of all electrons that have kinetic energies between T and $T+dT$. We call $y(T)$ the electron degradation spectrum. Under stationary irradiation it obeys the Spencer-Fano equation

$$nK_T y(T)+U(T)=0 , \tag{2}$$

where K_T is a linear operator discussed below, n is the number density of atoms in the medium, and $U(T)$ is the energy distribution of source electrons. In general, K_T is defined[13] such that $nK_T y(T)dT$ represents the net change in the number of electrons having energies between T and $T+dT$.

To discuss the K_T operator explicitly, we begin with the cross sections for all the processes involved. Let $\sigma_s(T)$ be the cross section for the excitation of the sth discrete state at excitation energy E_s by an electron of energy T. Let $d\sigma_{i\alpha}(T,E)/dE$ be the differential ionization cross section for the αth shell at energy transfer E, where I_α is the threshold; in other words, $[d\sigma_{i\alpha}(T,E)/dE]dE$ is the cross section for the ejection from the αth shell of an electron with kinetic energy between $E-I_\alpha$ and $E-I_\alpha+dE$. It is convenient to introduce the total ionization cross section for the αth shell

$$\sigma_{i\alpha}(T)=\int_{I_\alpha}^{(T+I_\alpha)/2} dE \frac{d\sigma_{i\alpha}(T,E)}{dE} , \tag{3}$$

and the total inelastic-scattering cross section

$$\sigma_{\rm tot}(T)=\sum_\alpha \sigma_{i\alpha}(T)+\sum_s \sigma_s(T) . \tag{4}$$

Furthermore, suppose that the ionization of the αth shell is followed by the production of an Auger electron of kinetic energy ε_α at the probability η_α. (We disregard the possibility of multiple Auger electrons, because we focus on the L-shell ionization of Ar.) Thus the K_T operator appropriate for the present work takes the form

$$\begin{aligned} K_T y(T)=&\sum_s \sigma_s(T+E_s)y(T+E_s)+\sum_\alpha \int_{I_\alpha}^{\lambda_\alpha} dE \frac{d\sigma_{i\alpha}(T+E,E)}{dE} y(T+E) \\ &+\sum_\alpha \int_{2T+I_\alpha}^{T_0} dT' \frac{d\sigma_{i\alpha}(T',T+I_\alpha)}{dE} y(T')+\sum_\alpha \eta_\alpha \delta(T-\varepsilon_\alpha)\int_{I_\alpha}^{T_0} dT' \sigma_{i\alpha}(T')y(T')-\sigma_{\rm tot}(T)y(T) . \end{aligned} \tag{5}$$

The symbol λ_α represents the smaller of $T+I_\alpha$ and T_0-T. The sum over the Auger terms obviously runs over inner shells only.

If the incident electrons are monoenergetic at T_0, we set $U(T)=\delta(T-T_0)$ and write the corresponding solution as $y(T_0,T)$. The ionization yield of the αth shell resulting from a single incident electron with energy T_0 is calculated as

$$N_{i\alpha}(T_0)=n\int_{I_\alpha}^{T_0} dT\, y(T_0,T)\sigma_{i\alpha}(T) . \tag{6}$$

Tne yield $N_s(T_0)$ of the excited state s is calculated similarly; one merely replaces $\sigma_{i\alpha}(T)$ with $\sigma_s(T)$ in Eq. (6).

Fowler equation

The Fowler equation for the total ionization yield $N_i(T)=\sum_\alpha N_{i\alpha}(T)$, viz., the mean number of ions produced as a result of complete degradation of an electron of energy T, is

$$K_T^\dagger N_i(T)+\sigma_i(T)=0 , \tag{7}$$

where $K_T^\dagger$ is the adjoint of the operator K_T and $\sigma_i(T)=\sum_\alpha \sigma_{i\alpha}(T)$ is the total ionization cross section. The operator $K_T^\dagger$ is represented explicitly as

$$\begin{aligned} K_T^\dagger N_i(T)=&\sum_s \sigma_s(T)N_i(T-E_s)+\sum_\alpha \int_{I_\alpha}^{(T+I_\alpha)/2} dE \frac{d\sigma_{i\alpha}(T,E)}{dE}[N_i(T-E)+N_i(E-I_\alpha)] \\ &+\sum_\alpha \sigma_{i\alpha}(T)\eta_\alpha \Theta(T-I_\alpha)N_i(\varepsilon_\alpha)-\sigma_{\rm tot}(T)N_i(T) , \end{aligned} \tag{8}$$

where $\Theta(x)=1$ for $x>0$ and $\Theta(x)=0$ otherwise.

In general, $N_i(T)$ is almost proportional to T at sufficiently high T, and therefore it is customary to express the ionization yield in terms of $W(T)=T/N_i(T)$, i.e., the mean energy for an ion pair.

Statistical fluctuations

There are several ways to evaluate the fluctuations. The most transparent among them is the method of Refs. 5 and 6, which uses the degradation spectrum as a basis. The variance $D(T)$ of the ionization yield satisfies an equation similar to the Fowler equation,

$$K_T^\dagger D(T)+\rho_i(T)=0 , \tag{9}$$

whose inhomogeneous term is expressed as

$$\begin{aligned} \rho_i(T)=&\sum_s \sigma_s(T)[N_i(T)-N_i(T-E_s)]^2 \\ &+\sum_\alpha \int_{I_\alpha}^{(T+I_\alpha)/2} dE \frac{d\sigma_{i\alpha}(T,E)}{dE} \\ &\times[N_i(T-E)+N_i(E-I_\alpha)+\eta_\alpha\Theta(T-I_\alpha)N_i(\varepsilon_\alpha)+1-N_i(T)]^2 , \end{aligned} \tag{10}$$

i.e., a generalization of the result of Refs. 5 and 6. The right-hand side of the above equation represents the change in the mean-squared number of ions in a single inelastic collision of an electron with energy T. The variance $D(T)$ can be expressed in the same form as Eq. (6), namely,

$$D(T)=n\int dT' y(T,T')\rho_i(T') . \quad (11)$$

Once we obtain the variance $D(T)$, we can readily calculate the Fano factor, $F(T)$, as given by Eq. (1).

METHOD OF NUMERICAL CALCULATIONS

We solve Eq. (2) directly by using the mesh size of 1 eV above 20 eV and 0.5 eV below 20 eV for the yield calculation. These mesh sizes are finer than those used by Douthat.[15] The recent development of supercomputers such as the Cray 2 allows us to use the finer mesh size, in order to look for the fine structure of the electron degradation spectra. The calculation time to solve Eq. (2) by the Cray 2 at an incident energy of 2 keV is within several minutes.

RESULTS AND DISCUSSIONS

Throughout the present work we consider incident electrons of energies $T_0 \leq 2000$ eV. Therefore, the K-shell ionization, whose threshold is 3.2 keV in Ar, need not be considered. The L-shell ionization (with threshold $I_L=250$ eV) and the M-shell ionization (with threshold $I_M=15.76$ eV) are both included in the calculations. In other words, the index α in Eqs. (3)–(5) represents either L or M. For the Ar L shell we may set the Auger probability at unity and the Auger electron energy ε_L at 200 eV. It should be noted that a measured LMM Auger spectrum[16] of Ar shows four main components of lines between 200 and 210 eV in addition to a large number of satellite lines down to 150 eV with total intensity of several percent. Thus our schematization of the Auger process using a single line is justifiable within a few eV.

We treat Ar gas at a pressure of 1 atm (i.e., 101 325 Pa) and at a temperature of 0 °C. Results can be readily converted to other densities, in the absence of appreciable dimers or other clusters in their ground state.

The degradation spectrum

Figure 1 shows the degradation spectrum when an electron with incident energy of 2 keV enters the Ar gas. The solid curve is the result of full calculations that include Auger electrons from the L-shell ionization, and the dashed curve represents the result of calculations that neglect the Auger electrons. The dashed curve is identical with the solid curve above 200 eV, because the kinetic energy of the Auger electrons is taken as 200 eV.

The degradation spectrum decreases rapidly near the source energy, and then it decreases gradually, having a minimum at about 300 eV. The degradation spectrum has a sharp spike at 200 eV that is due to the Auger effect, the increases like a step function below 190 eV. It starts increasing again as the energy decreases below 150 eV. The degradation spectrum has a slight shoulder around 15 eV; this is due to a peak of the cross section for the excitation of metastable states.

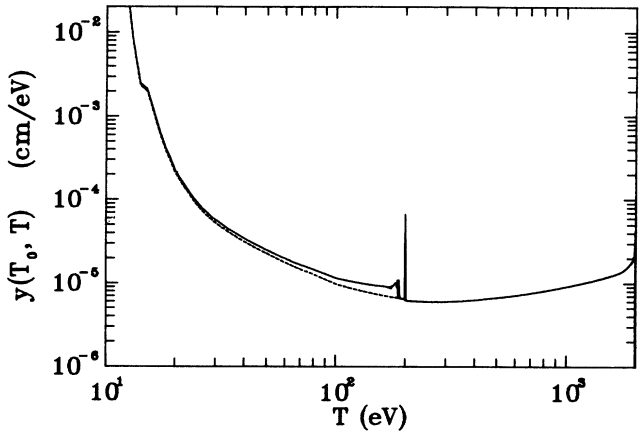

FIG. 1. Electron-degradation spectrum in Ar at a pressure at 1 atm and at a temperature of 0 °C for incident electron energy $T_0=2000$ eV, plotted as a function of electron energy T. The solid curve represents the result of the full calculation. The structures around $T=200$ eV originate when the Auger electrons follow the L-shell ionization. Indeed, calculations neglecting the Auger electrons give the result represented by the dashed curve, which differs from the solid curve below $T=200$ eV.

Figure 2 is an enlargement of the degradation spectrum near the source energy. The degradation spectrum shows oscillations near the incident energy due to the small number of collision processes involved. These oscillations are called the Lewis effect.[17] The Lewis effect in the helium gas caused by an energetic electron was discussed by Douthat[15] and by Kowari and Sato.[18] A Lewis effect in subexcitation electrons in nitrogen gas was also discussed by Kowari *et al.*[19] Characteristics of structures in the degradation spectrum are the following: The first discrete peak near the source energy is due mainly to the 11.72-eV excitation. The peak is modified slightly by

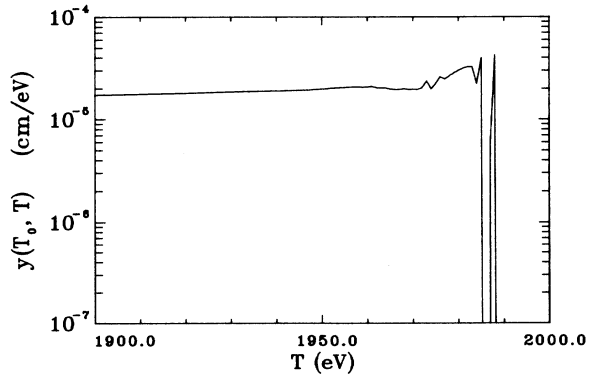

FIG. 2. Degradation spectrum near the source energy $T_0=2000$ eV. This figure is an enlargement of a part of Fig. 1 near T_0 and shows the Lewis effect.

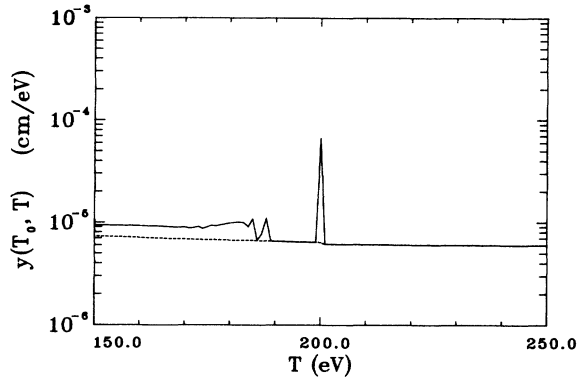

FIG. 3. Electron-degradation spectrum near 200 eV. This figure is an enlargement of a part of Fig. 1. The solid curve represents the result of the full calculation and the dashed curve the result of calculations without the Auger electron contributions.

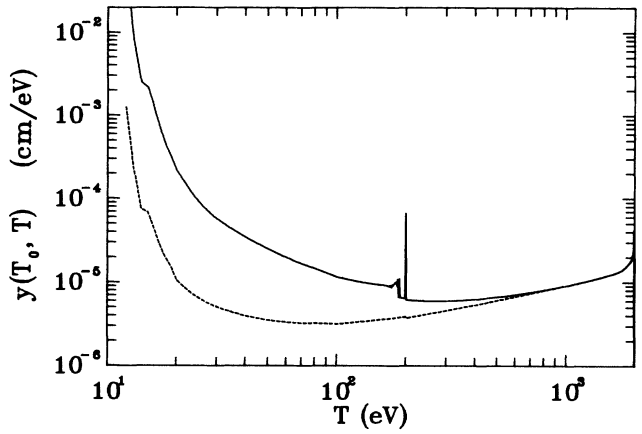

FIG. 4. Electron-degradation spectrum and the contribution by the primary electron. The solid curve is the same as in Fig. 1 and shows the full spectrum. The dashed curve represents the contribution to the spectrum by the degrading primary electron only. The difference between the two curves thus represents the contribution by secondary electrons and electrons of higher generations.

the 13.0-eV excitation, which gives rise to a shoulder on the left-hand side. The 12.0-eV excitation does not contribute to this peak because its cross section is appreciable only below 70 eV. The second peak is attributable to the contributions from the excitation of the 14.25- and 14.97-eV states. Structures in the degradation spectrum at 1984 eV are due to ionization and excitation (15.48 eV) by electrons at the source energy. The degradation spectrum between 1987 and 1977 eV reflects the shape of the differential cross section for ionization by electrons at the source energy. Two peaks between 1977 and 1970 eV are due to the second inelastic collisions of the initial electrons. The degradation spectrum becomes smooth below 1960 eV.

Figure 3 is an enlargement of the degradation spectrum around 200 eV to show more closely the influence of the Auger effect. The sharp peak (like a δ function) at 200 eV is due to the Auger electrons. The general shape of the degradation spectrum around 200 eV is similar to that near the source energy, because the ejection of Auger electrons amounts to a secondary source. The oscillatory structures around 190 eV show a Lewis effect due to the Auger electrons. The dashed curve results if we neglect the Auger electrons; hence, the difference between the two curves represents the contribution of the Auger electrons. This difference becomes smaller as the energy decreases, as is seen in Fig. 1. The Auger electron contribution becomes less visible at lower energies where it is overwhelmed by secondary electrons from the M-shell ionization.

The importance of secondary electrons

For the interpretation of the degradation spectrum it is necessary to study the role of each generation of electrons. For this purpose, we have carried out two sets of calculations: (i) the full solution $y(T_0, T)$ of the Spencer-Fano equation, i.e., calculations including primary- and secondary-electron terms [the second and third terms, respectively, in Eq. (3)]; and (ii) calculations neglecting the secondary-electron term and the Auger term. We denote the result of the latter calculations as $y^{(1)}(T_0, T)$, the superscript (1) indicating the first generation.

Figure 4 depicts two degradation spectra $y(T_0, T)$ and $y^{(1)}(T_0, T)$. From the source energy to about 1000 eV, the two degradation spectra are identical because no secondary electron is generated at $T > (T_0/2 - I_\alpha)$. However, below this energy, $y^{(1)}(T_0, T)$ is obviously smaller than $y(T_0, T)$, and the difference between the two grows progressively at lower energies. Furthermore, $y(T_0, T)$ shows a sharp spike at 200 eV corresponding to the Auger electrons, while $y^{(1)}(T_0, T)$ misses the spike since no Auger effect is included. Below this energy, these two degradation spectra show quite distinctive features. Specifically, $y(T_0, T)$ sharply increases as energy decreases, while $y^{(1)}(T_0, T)$ slowly decreases, reaches a shallow minimum at 100 eV, and resumes an increasing trend below this energy. The discrepancy between the two corresponds to a factor of about 3.5 at 100 eV and to a factor as large as 9.0 at 40 eV. This result means that more secondary electrons and higher-generation electrons are present at lower energies.

This discrepancy certainly influences yield calculations. While the ionization yield at high energies is rather insensitive to the secondary-electron contribution because the direct ionization dominates, excited-state yields are very sensitive because they include larger contributions from low-energy electrons. Indeed, neglecting the contribution of secondary electrons, one recovers about 65% of the total ionization yield, but only 2.9% of the yield of optically forbidden excitation, both for $T_0 = 2000$ eV. These results are consistent with the results of Kimura and Inokuti[10] based on the Fowler equation.

The ionization yield

In Table I, we show the total ionization yield as well as separate contributions from the M shell and the L shell,

TABLE I. Energy dependence of the ionization yield.

T (eV)	W value (eV)	Number of all ions	Number of M-shell ions	Number of L-shell ions
100	30.9	3.24	3.24	0
200	28.8	6.95	6.95	0
300	28.0	10.7	10.7	0.00216
500	27.5	18.2	18.2	0.0304
1000	27.2	36.8	36.6	0.169
1500	27.1	55.4	55.0	0.355
2000	27.0	74.0	73.4	0.573

calculated from the Spencer-Fano equation. At 2000 eV the present calculation yields the W value of 27.0 eV, which agrees very well with the previous result of 26.8 eV reported by Eggarter[8] and based on the Fowler equation.

An Auger effect follows the L-shell ionization. Resulting Auger electrons with the energy of 200 eV join in the further degradation processes. Let us consider the relative importance of the M shell and the L shell. In Table I we see that $N_{iM}(T) \gg N_{iL}(T)$ at all T; at $T=2000$ eV, for instance, $N_{iL}(T)$ amounts to 0.8% of the total. However, the consequences of the L-shell ionization are more important than this small percentage might suggest. The L-shell ionization causes an Auger effect, by which an electron of 200 eV is emitted. As is seen in Table I, an incident electron of $T=2000$ eV produces 0.573 L-shell ionizations on the average, and each Auger electron of 200 eV subsequently produces 6.95 M-shell ionizations. Thus Auger electron contributions to the M-shell ionizations amount to $0.573 \times 6.95 = 3.98$ per 2000-eV incident electron. This figure is included in the value $N_{iM}(2000 \text{ eV}) = 73.4$, obtained from the full solution of the Spencer-Fano equation. The amount 3.98 corresponds to 5.4% of the total $N_i(2000 \text{ eV})$.

Note that $N_{iL}(T)$ decreases rapidly as T approaches the L-shell threshold; this is a result of the energy dependence of $\sigma_{iL}(T)$. Even when one takes into account the Auger electron contributions, the role of the L-shell ionization is hardly noticeable in the total $N_i(T)$ at $T \leq 500$ eV. Consequently, $N_i(T)$ is a smooth function of T near the L-shell threshold. This observation is fully consistent with Combecher's measurements[20] on the total ionization yield of argon by electrons.

In measurements of the total ionization yield of hydrocarbons *by monoenergetic photons,* Suzuki and Saito[21] found structures with magnitudes amounting to several percent near the K-shell threshold of carbon. This is because the K-shell photoionization cross section rises abruptly above the threshold. Our result for the electron incidence is not inconsistent with the findings of Suzuki and Saito.

To discuss contributions from various T to the ionization yield as given by Eq. (6), it is useful to plot $nTy(T_0,T)\sigma_{i\alpha}(T)$ as a function of T. We call this plot the yield spectrum. Figure 5 is an example. The area under the curve in any energy interval represents contributions to the yield from that interval. The yield spectrum for the M-shell ionization rapidly decreases near the source energy, then gradually decreases with decreasing energy and shows a sharp peak at 200 eV that is due to the Auger electrons. The peak is accompanied by fine structures extending to about 190 eV because of a Lewis effect of the Auger electrons. The yield spectrum is slightly higher below the peak than above because of the contribution of the Auger electrons, and it is almost constant until the energy reaches the M-shell threshold. As is clear, about an equal amount of ionization is generated above 400 eV and below. As a qualification, note that the simplified representation of the Auger spectrum overemphasizes the fine structure. The use of many-line spectrum would have led to a smoother behavior of the yield spectrum.

The yield spectrum for the L-shell ionization (shown in the dashed line) monotonically decreases from the source energy to the L-shell ionization threshold, and it is similar in shape to that of the M-shell ionization in the same energy range. However, the magnitude of the L-shell ionization is much smaller than that of the M-shell ionization. Two-thirds of the yield is generated above 1000 eV and almost none near the L-shell ionization threshold. The yield spectrum for the L-shell ionization is surprisingly similar in shape to that estimated by Durup and

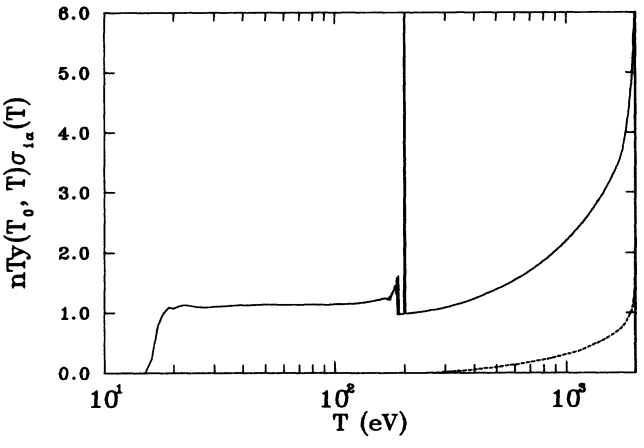

FIG. 5. Yield spectrum for ionization. The vertical axis represents the product $nTy(T_0,T)\sigma_{i\alpha}(T)$ and the horizontal axis the electron energy T on a logarithmic scale. Therefore the area under the curve corresponds to the contribution to the ionization yield from any interval of T. The solid curve represents the result of the full calculation. The dashed curve represents contributions of the L-shell ionization, multiplied by a factor of 10 so as to be discernible in this figure.

Platzman,[22] who treated, however, mainly the K shell of atoms other than argon. This is attributable to the gradual rise of inner-shell ionization cross sections just above the threshold.

The energy dependence of the W value

Figure 6 shows the energy dependence of the W value. This figure is in effect a reproduction of the calculations by Eggarter,[8] who used the Fowler equation. Here, we show comparison of the calculations with the experiment by Combecher.[20] The calculation is in excellent agreement with the experiment except for the region from 18 to 27 eV. The theoretical W value decreases rapidly above the ionization threshold as the energy increases and has a minimum at 20 eV. Then it rises again, peaking at 28 eV, and thereafter shows a gradual decrease beyond 30 eV. This is understood as follows. Near the ionization threshold, the ionization cross section is very small, and thus the ionization yield is very low; in turn, this results in the very large W value. As the energy increases, the ionization cross section increases rapidly, and as a result the W value decreases. At slightly higher energies the competition between ionization and excitation leads to the minimum around 20 eV. When the incident energy is above 28 eV, the incident electron ionizes the gas in two ways: (i) by the ionization in the first collision, and (ii) by the ionization after the electronic excitation. This makes the ionization yield larger, and hence the W value is lower. Precisely at 28 eV, the W value has a maximum. In the experimental result, we see a shoulder that most likely corresponds to the structures in the calculated result.

The Fano factor

Figure 7 shows $\rho_i(T)$ as a function of energy T. The solid curve represents the result of the full calculation including the Auger electrons. The function $\rho_i(T)$ increases rapidly with $T \geq I_M$ and shows several oscillations between 25 and 70 eV. The occurrence of these oscillations is understandable from the structure of the defining expression for $\rho_i(T)$, Eq. (10).

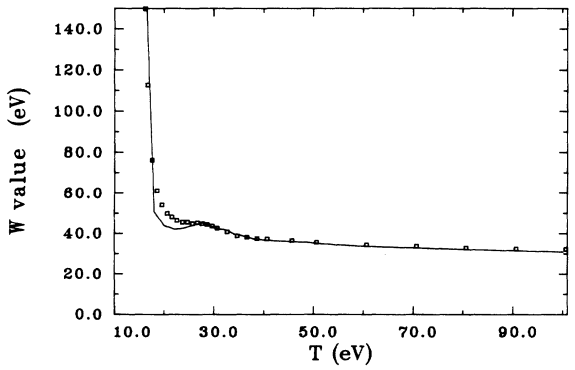

FIG. 6. W value plotted as a function of incident electron energy T. The solid curve shows the result of the present calculations. The squares show the result of measurements by Combecher (Ref. 20).

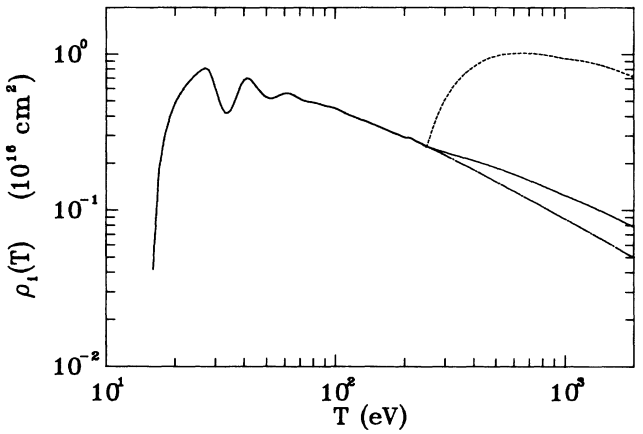

FIG. 7. Function $\rho_i(T)$ as a function of electron energy T. The function $\rho_i(T)$ is defined by Eq. (10) of the text and signifies the contribution of collisions of electrons at energy T to the variance in the ionization yield. The solid curve represents the result of the full calculation. The chain-dashed curve represents the results of calculations without the contributions from the L-shell ionization. The dashed curve represents the results of calculations without the contributions of the Auger electrons.

For 15.8 eV $< T <$ 28 eV, only $N_i(T)$ is nonvanishing on the right-hand side of Eq. (10). For 28 eV $< T <$ 32 eV, $N_i(T-E_s)$ also is nonvanishing; thus $\rho_i(T)$ abruptly drops at $T=28$ eV. At $T > 2I_M = 32$ eV, $N_i(T-E)$ also becomes nonzero, and this leads to a rapid increase in $\rho_i(T)$. The reason for the increase, rather than a decrease, is that $1-N_i(T)>0$ at $T<37$ eV and hence $N_i(T-E)$ and $1-N_i(T)$ are genuinely additive. Consequently, the minimum occurs at $T=32$ eV.

Above 40 eV, $\rho_i(T)$ begins to decrease again. This is so because the difference $N_i(T)-N_i(T-E_s)$ is an increasing function of T at $T<40$ eV but is virtually constant at $T>40$ eV; this arises from the T dependence of $N_i(T)$, as is seen in Fig. 5 of Eggarter.[9]

Above 50 eV, $\rho_i(T)$ begins to increase once again. This increase is due to the $N_i(E-I_M)$ term, which begins to be nonvanishing when T reaches $3I_M$. The increasing trend eventually terminates at $T>60$ eV, where the quantity $N_i(T-E)+N_i(E-I_M)+1-N_i(T)$ becomes almost constant. At higher T, the T dependence of $\rho_i(T)$ is chiefly governed by the T dependence of the cross sections, which gradually decline according to the Bethe form $T^{-1}\ln(\text{const}\times T)$. Thus we understand the gradual decline of $\rho_i(T)$ above 60 eV.

Above 250 eV, L-shell ionization is possible. Although the L shell contributes modestly to the total ionization yield, it greatly influences $\rho_i(T)$, and hence the Fano factor, because of large energy transfers involved. To see the L-shell effects clearly, we have carried out calculations on two hypothetical cases. In calculation I, we disregard the production of Auger electrons; in other words, we set $\eta_L = 0$ in Eqs. (5), (8), and (10). In calcula-

tion II, we disregard the L-shell effect altogether; in other words, we set all of the L-shell cross sections at zero in Eqs. (5), (8), and (10).

Calculations I and II differ from full calculations at $T > I_L = 250$ eV. As is seen in Fig. 7, the result of calculation I (shown by the dashed curve) departs markedly from that of the full calculation; it rises rapidly above 250 eV and flattens around 700 eV. The gross overestimate of $\rho_i(T)$ in calculation I comes from the large magnitude of the quantity $N_i(T-E)+N_i(E-I_L)+1-N_i(T)$ for the L-shell ionization. In the full calculation, the same quantity certainly appears, but it is almost canceled by the Auger electron term $\Theta(T-I_L)N_i(\varepsilon_L)$.

The values of $\rho_i(T)$ from calculation II (shown by the chain-dashed curve in Fig. 7) are somewhat lower than the values from the full calculation. This is readily understandable because calculation II disregards the L-shell ionization, which is accompanied by large energy losses.

Figure 8 shows the energy dependence of the Fano factor. The Fano factor at the ionization threshold is unity, as is always the case. The reason is that the probability of ionization $\sigma_i(T)/\sigma_{\text{tot}}(T)$ vanishes at the threshold and that the ionization process therefore satisfies the Poisson statistics. The Fano factor thereafter decreases rapidly until energy reaches 36 eV. In the energy range $I \le T \le I + E_s$, Eq. (1) reduces precisely to the equation[5,6]

$$F(T)=\rho_i(T)/\sigma_i(T) . \tag{12}$$

As is shown in Figs. 7 and 9, $\rho_i(T)$ increases less rapidly than $\sigma_i(T)$ near I_M, and therefore $F(T)$ decreases according to Eq. (12). Since $\sigma_i(T)$ is rather smooth above 28 eV, the Fano factor reproduces the oscillatory structures in $\rho_i(T)$.

Figure 8 also shows results from calculations I and II. The result from the full calculation shows a gradual increase with energy T above 500 eV, which is absent in the result of calculation II. The increase is clearly attributable to the increase of $\sigma_{iL}(T)$ with T. The result from calculation I shows a pronounced rise at $T > 250$ eV, which is entirely unrealistic. By contrast, calculation II gives results much closer to the full results. All these findings are consequences of the behavior of $\rho_i(T)$.

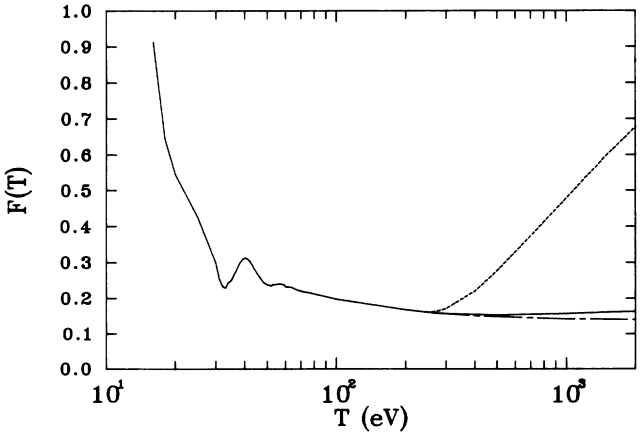

FIG. 8. Fano factor $F(T)$ as a function of electron energy T. The solid curve represents the result of the full calculation. The chain-dashed curve represents the result of calculations without the L-shell contribution. The dashed curve represents the result of calculations without Auger electron contributions.

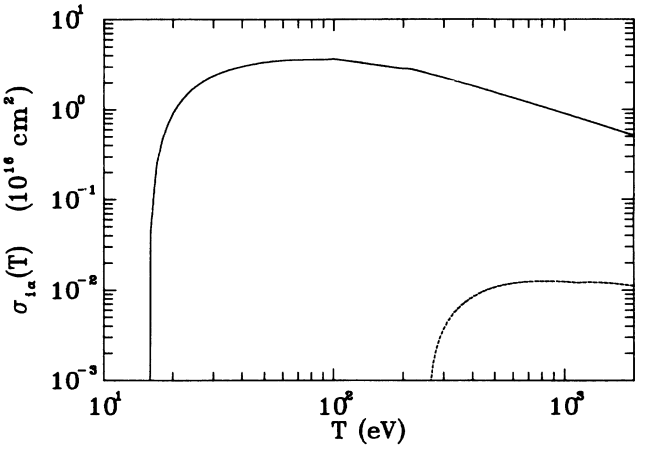

FIG. 9. Ionization cross section plotted as a function of electron energy T. The solid curve represents the M-shell ionization cross section of Ar. The dashed curve represents the L-shell ionization cross section.

Figure 10 shows the variance spectrum, viz., $nTy(T_0,T)\rho_i(T)$ as a function of T on a logarithmic scale. The area under the curve over any interval of T represents the contribution to the variance $D(T_0)$ from that interval. With decreasing energy, the variance spectrum decreases rather rapidly near the source energy,

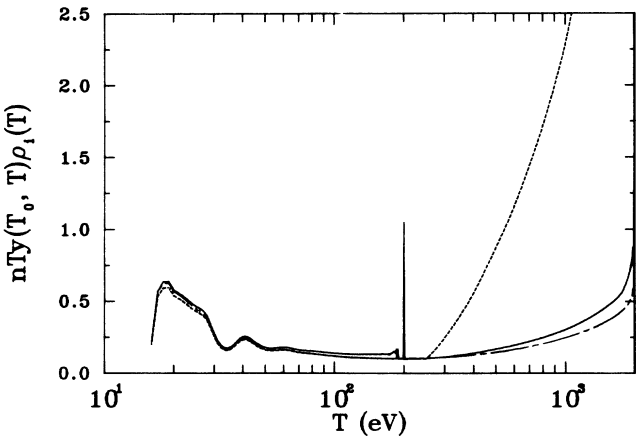

FIG. 10. Variance spectrum. The vertical axis represents the product $nTy(T_0,T)\rho_i(T)$, which shows the contribution to the variance $D(T_0)$ from electron energy T, and the horizontal axis represents the electron energy T on a logarithmic scale. The solid curve represents the result of the full calculation. The chain-dashed curve represents the result of calculations excluding the L-shell contribution. The dashed curve represents the result of calculations without the Auger electron contributions.

TABLE II. The energy dependence of the Fano factor in Ar.

T (eV)	$F(T)$
20	0.547
30	0.297
50	0.237
70	0.220
100	0.197
200	0.167
300	0.156
400	0.153
700	0.155
1000	0.157
1500	0.161
2000	0.163

then gradually becomes almost flat at 300 eV. A structure due to the Auger electrons between 180 and 200 eV has the same shape as that of the yield spectrum (Fig. 5). The variance spectrum shows oscillations below 70 eV because of the oscillations of $\rho_i(T)$. Below 30 eV, it rises rapidly, has a peak at 18 eV, and drops near I_M.

The three curves are distinct below 200 eV, because the values of $y(T_0,T)$ from the three calculations are different [although $\rho_i(T)$ values are common to the three calculations]. The variance spectrum from calculation II rises excessively at high T as a result of the behavior of $\rho_i(T)$ (seen in Fig. 7).

To facilitate close examination, we present in Table II the values of the Fano factor obtained from the full calculation. Our results are in good agreement with data in the literature, both theoretical and experimental. First, we discuss comparison with other theoretical results. Alkhazov and co-workers[23,24] used the approximate expression of Fano[25] and obtained 0.16 at 1576 eV, in good agreement with our value 0.161 at 1500 eV. The results of Monte Carlo simulations[1,3] are within 5% of our values at $T \geq 1000$ eV. In particular, the results by Unnikrishnan and Prasad[1] closely agree with ours in the entire energy region $T \leq 2000$ eV. This is not surprising because both they and we used as input virtually the same cross-section data as that presented by Eggarter.[8] The results by Grosswendt[3] are somewhat higher than ours at $T < 1000$ eV, probably because different cross-section data were used.

As for experiments, Neumann[26] reported the value 0.14 ± 0.02 for electrons of energies 260–2820 eV, which is consistent with our results. There seems to be no experimental report on precise energy dependence of the Fano factor.

Kase *et al.*[27] used 5.3-MeV α particles and obtained the Fano factor of $0.20^{+0.01}_{-0.02}$ for pure argon. It is not immediately clear whether this result is consistent with our values, because α particles degrade differently from electrons. One may tentatively compare the result of Kase *et al.* with our result of 0.155 for electrons of 700 eV, which have the same speed as the 5.3-MeV α particles. In this respect we note that for W values there are only small differences between electrons (above several hundred eV) and α particles (above several MeV) as fully documented in the International Commission Radiation units (ICRU) report.[28]

For closer examination one must consider both the direct ionization by the α particles and the indirect ionization by secondary electrons. In general these two are roughly comparable in magnitude. Indeed, Sato *et al.*[29] shows that the direct ionization of He by 5-MeV α particles is about 61% of the total ionization. In order to calculate precisely the Fano factor for the α-particle incidence, it is necessary to generalize the basic theory as outlined in the second section. This is the theme of another article under preparation.[30] According to the full analysis, the Fano factor for an α particle should be somewhat larger than that for an electron of the same speed. Consequently, the present results are consistent with the measurements by Kase *et al.*[27]

CONCLUDING REMARKS

Upon consideration of the effects of inner-shell ionization on electron degradation, it is important to account for the degradation of Auger electrons resulting from the inner-shell ionization. The neglect of the Auger electron effects leads to unrealistic results in various quantities and most notably in the Fano factor. A stringent test of our theoretical results will be measurements of the Fano factor for electrons at various energies below 1000 eV, and especially below 100 eV, where we predict nonmonotonic energy dependence.

The present study illustrates the effectiveness of the analytic transport theory in elucidating the rich physics of electron degradation phenomena (for instance, the reason for the energy dependence of the Fano factor), to greater depth than was seen in earlier studies.[1–3]

Finally, we plan to report on the spectrum of subexcitation electrons, which is obtained from the solution of the Spencer-Fano equation. A preliminary report[31] of the study on this topic has been published; a fuller account of the work is planned to appear.

ACKNOWLEDGMENTS

We thank U. Fano for valuable remarks on an earlier manuscript. Work supported by the U.S. Department of Energy, Office of Health and Environmental Research, under Contract No. W-31-109-Eng-38.

[1]K. Unnikrishnan and M. A. Prasad, Radiat. Res. **80**, 225 (1979).
[2]M. Parikh, J. Chem. Phys. **73**, 93 (1980).
[3]B. Grosswendt, J. Phys. B **17**, 1391 (1984).
[4]L. V. Spencer and U. Fano, Phys. Rev. **93**, 1172 (1954).
[5]A. R. P. Rau, M. Inokuti, and D. A. Douthat, Phys. Rev. A **18**, 971 (1978).
[6]M. Inokuti, D. A. Douthat, and A. R. P. Rau, Phys. Rev. A **22**, 445 (1980).
[7]M. Inokuti, M. A. Dillon, and M. Kimura, Int. J. Quantum

Chem. **21**, 251 (1987).
[8]E. Eggarter, J. Chem. Phys. **62**, 833 (1975).
[9]E. Eggarter, J. Chem. Phys. **84**, 6123 (1986).
[10]M. Kimura and M. Inokuti, J. Chem. Phys. **87**, 3875 (1987).
[11]M. A. Prasad and K. Unnikrishnan, Phys. Rev. A **23**, 2082 (1981).
[12]J. K. Knipp, T. Eguchi, M. Ohta, and S. Nagata, Prog. Theor. Phys. **10**, 24 (1953).
[13]M. Inokuti, M. Kimura, and M. A. Dillon, Phys. Rev. A **38**, 1217 (1988).
[14]E. Eggarter and M. Inokuti, Argonne National Laboratory Report No. ANL-80-58, 1980 (unpublished).
[15]D. A. Douthat, Radiat. Res. **61**, 1 (1975).
[16]L. O. Werme, T. Bergmark, and K. Siegbahn, Phys. Scr. **8**, 149 (1973).
[17]H. W. Lewis, Phys. Rev. **125**, 937 (1962).
[18]K. Kowari and S. Sato, Bull. Chem. Soc. Jpn. **54**, 2878 (1981).
[19]K. Kowari, M. Kimura, and M. Inokuti, J. Chem. Phys. **89**, 7229 (1988).
[20]D. Combecher, Radiat. Res. **84**, 189 (1980).
[21]I. H. Suzuki and N. Saito, Bull. Chem. Soc. Jpn. **60**, 2989 (1987).
[22]J. Durup and R. L. Platzman, Int. J. Radiat. Phys. Chem. **7**, 121 (1975).
[23]G. D. Alkhazov, Zh. Tekh. Fiz. **41**, 1949 (1971) [Sov. Phys.—Tech. Phys. **16**, 1995 (1972)].
[24]G. D. Alkhazov, A. P. Komar, and A. A. Vorob'ev, Nucl. Instrum. Methods **48**, 1 (1967).
[25]U. Fano, Phys. Rev. **72**, 26 (1947).
[26]W. Neumann, in *The Seventh Symposium on Microdosimetry, Oxford, U.K., 1980,* edited by J. Booz, H. G. Ebert, and H. D. Hartfield (Harwood Academic, London, 1981), p. 1067.
[27]M. Kase, T. Aioka, H. Mamyoda, J. Kikuchi, and T. Doke, Nucl. Instrum. Methods **227**, 311 (1984).
[28]International Commission on Radiation Units and Measurements, Report No. 31, 1979 (unpublished).
[29]S. Sato, K. Kowari, and K. Okazaki, Bull. Chem. Soc. Jpn. **49**, 933 (1976).
[30]M. Inokuti, K. Kowari, and M. Kimura (unpublished).
[31]M. Inokuti, M. Kimura, and K. Kowari, Chem. Phys. Lett. **152**, 504 (1988).